Synthesis, Crystal Structures, and Magnetostructural Correlations in Two New One-Dimensional Nickel(II) Complexes with Azido as Bridging Ligand. Effect of Temperature

Montserrat Monfort,*[1a] Joan Ribas,[1a] Xavier Solans,[1b] and Mercé Font-Bardía[1b]

Departament de Química Inorgànica, Universitat de Barcelona, Diagonal, 647, 08028 Barcelona, Spain, and Departament de Cristal.lografia, Mineralogia i Dipòsits Minerals, Universitat de Barcelona, Martí i Franqués, s/n, 08028 Barcelona, Spain

Received June 19, 1996[⊗]

Two new nickel(II) *trans*-monodimensional end-to-end azide-bridged complexes were synthesized and characterized: $[Ni(1,3\text{-diamino-}2,2\text{-dimethylpropane})_2(\mu\text{-}N_3)]_n(PF_6)_n$ (**1**) and $[Ni(1,3\text{-diaminopropane})_2(\mu\text{-}N_3)]_n(PF_6)_n$ (**2**). The crystal structures of **1** and **2** were solved. Complex **1** crystallizes in the orthorhombic system, space group *Pnmn* with $a = 18.046(6)$ Å, $b = 8.7050(12)$ Å, $c = 6.139(2)$ Å, and $Z = 2$. Complex **2** crystallizes in the orthorhombic system, space group *Pnmn* with $a = 15.186(3)$ Å, $b = 8.808(2)$ Å, $c = 5.983(2)$ Å, and $Z = 2$. In the two complexes, the chains run along the *c* axis and the nickel atoms are situated in similar distorted octahedral environments. The two complexes are very similar and may be described as one-dimensional systems with the azido bridging ligands in the *trans* position. The magnetic properties of the two compounds were studied by susceptibility measurements *vs* temperature. **1** and **2** show a discontinuity at 235 and 230 K, respectively, which may be attributed to a phase transition at these relatively high temperatures. The χ_M *vs* T plot for **1** and **2** show the typical shape for antiferromagnetically coupled nickel(II) one-dimensional complexes with a maximum near 35 (**1**) and 100 K (**2**), respectively. From the spin Hamiltonian $-J\Sigma S_i S_j$, *J* values for **1** and **2** were −41.1 and −70.6 cm^{-1} in the high-temperature zone and −19.4 and −55.8 cm^{-1} for the low-temperature range. This difference in magnetic behavior may be explained in terms of the phase transition, which changes the crystal parameters *a* and *b*, as has been shown from powder diffraction data. This transition changes the dihedral Ni−NNN−Ni angles (0° at room temperature) and should thus decrease the antiferromagnetic coupling, as is experimentally observed.

Introduction

The azido ion is a good bridging ligand, which easily coordinates Ni(II) ions, giving discrete polynuclear complexes in either end-to-end[2−5] (antiferromagnetic coupling) or end-on[6−12] (ferromagnetic coupling) form, one-dimensional systems in the two forms,[13−24] and, finally, one- or bidimensional complexes in which both end-to-end and end-on forms are present.[25] Focusing our interest on one-dimensional antiferromagnetic systems, we find that the complexes reported to date may present the two azido ligands in *trans*[13−21] or *cis*[17,22−24] position. In the first case the azido bridging ligand allows a very good pathway for the magnetic exchange via d_{z^2} orbitals; in the second case there are two possibilities for the magnetic pathway: $d_{xy}-d_{z^2}$ or $d_{xy}-d_{xy}$, which reduces the antiferromagnetic coupling, as experimentally observed.[22−24] Magnetostructural correlations have recently been reported[15,19] for systems of this kind, in which the *J* parameter (cm^{-1}) is well-correlated to the Ni−N−N angle and to the Ni−NNN−Ni torsion angle.

⊗ Abstract published in *Advance ACS Abstracts,* November 15, 1996.

(1) (a) Departament de Qúmica Inorgànica, University of Barcelona. (b) Departament de Crystallografia, University of Barcelona.
(2) Wagner, F.; Mocella, M. T.; D'Aniello, M. J.; Wang, A. J. H.; Barefield, E. K. *J. Am. Chem. Soc*. **1974**, *96*, 2625.
(3) Pierpont, C. G.; Hendrickson, D. N.; Duggan, D. M.; Wagner, F.; Barefield, E. K. *Inorg. Chem*. **1975**, *14*, 604.
(4) Chaudhuri, P.; Guttman, M.; Ventur, D.; Wieghardt, K.; Nuber, B.; Weiss, J. J. *J. Chem. Soc., Chem. Commun*. **1985**, 1618.
(5) Ribas, J.; Monfort, M.; Diaz, C.; Bastos, C.; Solans, X. *Inorg. Chem*. **1993**, *32*, 3557.
(6) Arriortua, M. I.; Cortés, A. R.; Lezama, L.; Rojo, T.; Solans, X. *Inorg. Chim. Acta* **1990**, *174*, 263.
(7) Escuer, A.; Vicente, R.; Ribas, J. *J. Magn. Magn. Mater*. **1992**, *110*, 181.
(8) Vicente, R.; Escuer, E.; Ribas, J.; El Fallah. M. S.; Solans, X.; Font-Bardía, M. *Inorg. Chem*. **1993**, *32*, 1920, and references cited therein.
(9) Cortés, R.; Ruiz de Larramendi, J. I.; Lezama, L.; Rojo, T.; Urtiaga, K.; Arriortua, M. I. *J. Chem. Soc., Dalton Trans*. **1992**, 2723.
(10) Ribas, J.; Monfort, M.; Costa, R.; Solans, X. *Inorg. Chem*. **1993**, *32*, 695.
(11) Escuer, A.; Vicente, R.; Ribas, J.; Solans, X. *Inorg. Chem*. **1995**, *34*, 1793.
(12) Halcrow, M. A.; Sun, J. S.; Huffman, J. C.; Christou, G. *Inorg. Chem*. **1995**, *34*, 4167.
(13) Vicente, R.; Escuer, A.; Ribas, J.; Solans, X. *Inorg. Chem*. **1992**, *31*, 1726.
(14) Escuer, A.; Vicente, R.; Ribas, J.; El Fallah, M. S.; Solans, X. *Inorg. Chem*. **1993**, *32*, 1033.
(15) Escuer, A.; Vicente, R.; Ribas, J.; El Fallah, M. S.; Solans, X.; Font-Bardia, M. *Inorg. Chem*. **1993**, *32*, 3727.
(16) Escuer, A.; Vicente, R.; El Fallah, M. S.; Ribas, J.; Solans, X.; Font-Bardía, M. *J. Chem. Soc., Dalton Trans*. **1993**, 2975.
(17) Escuer, A.; Vicente, R.; Ribas, J.; El Fallah, M. S.; Solans, X.; Font-Bardía, M. *Inorg. Chem*. **1994**, *33*, 1842.
(18) Ribas, J.; Monfort, M.; Diaz, C.; Bastos, C.; Solans, X. *Inorg. Chem*. **1994**, *33*, 484.
(19) Escuer, A.; Vicente, R.; Ribas, J.; El Fallah, M. S.; Solans, X.; Font-Bardía, M. *Adv. Mater. Res*. **1994**, *1−2*, 581.
(20) Vicente, R.; Escuer, A. *Polyhedron* **1995**, *14*, 2133.
(21) Vicente, R.; Escuer, A.; Ribas, J.; El Fallah, M. S.; Solans, X.; Font-Bardía, M. *Inorg. Chem*. **1995**, *34*, 1278.
(22) Cortés, R.; Urtiaga, K.; Lezama, L.; Pizarro, J. L.; Goñi, A.; Arriortua, M. L.; Rojo, T. *Inorg. Chem*. **1994**, *33*, 4009.
(23) Ribas, J.; Monfort, M.; Diaz, C.; Bastos, C.; Mer, C.; Solans, X. *Inorg. Chem*. **1995**, *34*, 4986.
(24) Ribas, J.; Monfort, M.; Ghosh, B. K.; Cortés, R.; Solans, X.; Font-Bardía, M. *Inorg. Chem*. **1996**, *35*, 864.
(25) (a) Monfort, M.; Ribas, J.; Solans, X. *J. Chem. Soc., Chem. Commun*. **1993**, 350. (b) Ribas, J.; Monfort, M.; Solans, X.; Drillon, M. *Inorg. Chem*. **1994**, *33*, 742. (c) Ribas, J.; Monfort, M.; Ghosh, B. K.; Solans, X. *Angew. Chem., Int. Ed. Engl*. **1994**, *33*, 2087. (d) Ribas, J.; Monfort, M.; Ghosh, B. K.; Solans, X.; Font-Bardía, M. *J. Chem. Soc., Chem. Commun.* **1995**, 2375.

S0020-1669(96)00733-1 CCC: $12.00

In a given synthesis it is impossible to predict which kind of complex (*trans* or *cis*) will be obtained. Working with 1,3-diaminopropane and its derivative 1,3-diamino-2,2-dimethylpropane, we were able to synthesize two new *trans* complexes: $[Ni(1,3\text{-diamino-2,2-dimethylpropane})_2(\mu\text{-}N_3)]_n(PF_6)_n$ (**1**) and $[Ni(1,3\text{-diaminopropane})_2(\mu\text{-}N_3)]_n(PF_6)_n$ (**2**), which were similar in their structure at room temperature, but both complexes showed an abrupt change in magnetic susceptibility at lower temperature, which may be attributed to a phase transition, manifested by differential scanning calorimetry (DSC) measurements and X-ray powder diffraction. The crystals of the two complexes were stable at room temperature but not at low temperature, so we were able to solve the crystal and molecular structure only at 293 K. This is the first case in which this change in magnetic susceptibility has been observed for these kinds of one-dimensional nickel−azido complexes, but it is frequent in dinuclear complexes with two end-on azido bridges.[11] The magnetic data at high and low temperatures have been correlated with structural parameters, confirming the importance of the nickel−azido angles and the nickel−azido−nickel torsion angle.

Experimental Section

Caution! Azido complexes of metal ions are potentially explosive. Only a small amount of material should be prepared, and it should be handled with caution.

Materials. Sodium azide, nickel(II) nitrate, potassium hexafluorophosphate, 1,3-diaminopropane, and 1,3-diamino-2,2-dimethylpropane (Aldrich) were used as received, without further purification.

Synthesis of the New Complexes. $[Ni(1,3\text{-diamino-2,2-dimethylpropane})_2(\mu\text{-}N_3)]_n(PF_6)_n$ (1). An aqueous solution of 1 mmol (0.065 g) of NaN_3 was added to an aqueous solution of 1 mmol (0.291 g) of $Ni(NO_3)_2{\cdot}6H_2O$ and 2 mmol (0.204 g) of 1,3-diamino-2,2-dimethylpropane in 30 mL of water. After filtration to remove any impurity, 1.2 mmol (0.220 g) of KPF_6 was added with continuous stirring. The aqueous solution was left undisturbed, and well-formed blue crystals of **1** were obtained after several days. The elemental analyses (C, N, H, Ni) were consistent with the formulation $C_{10}H_{28}F_6N_7NiP$. Anal. Calcd/found: C, 26.69/26.8; H, 6.27/6.3; N, 21.78/21.9; Ni, 13.05/13.0.

$[Ni(1,3\text{-diaminopropane})_2(\mu\text{-}N_3)]_n(PF_6)_n$ (2). The new complex was obtained as **1** by using 2 mmol (0.148 g) of 1,3-diaminopropane instead of 1,3-diamino-2,2-dimethylpropane. The elemental analyses (C, N, H, Ni) were consistent with the formulation $C_6H_{20}F_6N_7NiP$. Anal. Calcd/found: C, 18.29/18.3; H, 5.12/5.1; N, 24.89/24.9; Ni, 14.90/15.0.

Physical Measurements. IR spectra (4000−400 cm^{-1}) were recorded from KBr pellets in a NICOLET 520 FT-IR spectrometer. Magnetic measurements were carried out on polycrystalline samples (30−40 mg) with a pendulum type magnetometer−susceptometer (MANICS DSM.8) equipped with an Oxford Helium continuous flow cryostat, working in the 4.2−300 K range, and a Drusch EAF 16UE electromagnet. The magnetic field was approximately 1.2 T. These measurements were also repeated with a Quantum Design MPMS SQUID susceptometer operating at a magnetic field of 0.5 T between 2 and 300 K. The diamagnetic corrections were evaluated from Pascal's Tables.

Crystal Data Collection and Refinement. Crystals (0.20 × 0.10 × 0.10 mm) of **1** and (0.3 × 0.1 × 0.1 mm) of **2** were selected and mounted on an ENRAF-NONIUS CAD4 four-circle diffractometer for **1** and on a Philips PW-1100 four-circle diffractometer for **2**. Unit cell parameters were determined from automatic centering of 25 reflections [($12 \le \theta \le 21°$) for **1** and $8 \le \theta \le 16°$ for **2**] and refined by least-squares method. Intensities were collected with graphite monochromatized Mo Kα radiation, using the $\omega/2\theta$ scan technique. For **1** 1490 reflections were measured in the range $2.26 \le \theta \le 29.95°$, 1170 of which were assumed as observed when applying the condition $I \ge 2\sigma(I)$. For **2** 1274 reflections were measured in the range $3.66 \le \theta \le 29.90°$, 589 of which were assumed as observed when applying the same condition. Three reflections were measured every 2 h as orientation and intensity control; significant intensity decay was not observed. Lorentz−polarization corrections but not absorption corrections were made. The crystallographic data are gathered in Table 1. The crystal structures were solved by Patterson synthesis using the SHELXS computer program[26] and refined by the full-matrix least-squares method, using the SHELX76[27] computer programs. The function minimized was $\Sigma w[|F_o|^2 - |F_c|^2]^2$, where $w = [\sigma^2(I) + (k_1P)^2 + k_2P]^{-1}$ and $P = (|F_o|^2 + 2|F_c|^2)/3$; the values of k_1 and k_2 are respectively 0.1343 and 0.2558 for **1** and 0.1634 and 0 for **2**. *f*, *f*′, and f″ were taken from the *International Tables of X-ray Crystallography*.[28] For both complexes all H atoms were computed and refined with an overall isotropic temperature factor, using a riding model. For **2**, fluorine atoms of PF_6^- were located in disordered position; an occupancy factor of 0.5 was assigned according to the height of the Fourier synthesis. For **1** the final *R* factor was 0.066 ($R_w = 0.097$) for all observed reflections. A set of 72 parameters was refined: maximum shift/esd = 0.07; maximum and minimum peaks in final difference synthesis were +0.5 and −0.4 e $Å^{-3}$, respectively. For **2** the final *R* factor was 0.068 ($R_w = 0.096$) for all observed reflections. A set of 133 parameters was refined: maximun shift/esd = 0.12; maximum and minimum peaks in final difference syntheses were +0.5 and −0.3 e $Å^{-3}$, respectively. Final atomic coordinates are given in Table 2.

Table 1. Crystallographic Data for **1** and **2**

	1	**2**
chem formula	$C_{10}H_{28}N_7Ni{\cdot}PF_6$	$C_6H_{20}N_7Ni{\cdot}PF_6$
fw	450.07	393.97
space group	*Pnmn*	*Pnmn*
T (°C)	293	293
a (Å)	18.046(6)	15.186(3)
b (Å)	8.7050(12)	8.808(2)
c (Å)	6.139(2)	5.983(2)
α (deg)	90	90
β (deg)	90	90
γ (deg)	90	90
V ($Å^3$)	964.4(3)	800.3(4)
Z	2	2
λ (Å)	0.710 69	0.710 69
ρ_{calcd} (g cm^{-3})	1.550	1.635
μ (mm^{-1})	1.153	1.376
$R(F_o)^a$	0.066	0.068
$R_w(F_o)^b$	0.097	0.096

^{a} $R(F) = [\sum||F_o| - |F_c||]/\sum|F_o|$. ^{b} $R_w = [\sum w||F_o|^2 - |F_c|^2|]/\sum w|F_o|^2$.

Results and Discussion

Description of the Structures. The two structures consist of 1-D nickel−azido chains propagated along the *c* axis and isolated by PF_6^- anions, found in the interchain space. In the chain structures, each Ni(II) atom is coordinated by two bidentate 1,3-diamino-2.2-dimethylpropanes for **1** and 1,3-diaminopropanes for **2** and two azido ligands in a distorted octahedral *trans* arrangement.

$[Ni(1,3\text{-diamino-2,2-dimethylpropane})_2(\mu\text{-}N_3)]_n(PF_6)_n$ (1). A labeled scheme is shown in Figure 1. The main bond lengths and angles are listed in Table 3. Other distances and angles may be found in the Supporting Information. The nickel atom occupies a distorted octahedral environment, formed by two N atoms of the azido bridging ligands at 2.125 Å and four N atoms of the two bidentate amine ligands at the same distance, 2.108 Å, giving a local D_{4h} symmetry. The most important data from a magnetic point of view are the Ni−N(1)−N(2) angle and the dihedral Ni−NNN−Ni torsion angle. These angles are 136.5 and 0°, respectively.

(26) Sheldrick, G. M. *Acta Crystallogr*. **1990**, *A*46, 467.
(27) Sheldrick,G. M. *SHELX*, A computer program for crystal structure determination; University of Cambridge: Cambridge, England, 1976.
(28) *International Tables for X-ray Crystallography*; Kynoch Press: Birmingham, England, 1976.

Table 2. Atomic Coordinates ($\times 10^4$) and Equivalent Isotropic Displacement Parameters (2×10^3) for **1** and **2**[a]

	x	*y*	*z*	*U*(eq)
		Complex **1**		
Ni	0	0	0	31(1)
P	0	−5000	−5000	52(1)
N(1)	305(3)	0	3344(5)	52(1)
N(2)	0	0	5000	38(1)
N(4)	−793(2)	−1743(4)	494(5)	42(1)
C(1)	−1466(2)	−1460(5)	1812(6)	57(1)
C(2)	−1903(3)	0	1185(9)	49(1)
C(4)	−2095(4)	0	−1211(11)	74(2)
C(5)	−2605(4)	0	2639(15)	86(3)
F(1)	−456(3)	−3649(8)	−3994(18)	189(3)
F(2)	−602(7)	−5000	−6819(15)	184(4)
		Complex **2**		
Ni	0	0	0	47(1)
P	0	5000	5000	65(1)
N(1)	−453(8)	0	3355(13)	87(3)
N(2)	0	0	5000	85(5)
N(4)	919(4)	1720(8)	681(15)	88(2)
C(1)	1825(8)	1407(16)	915(26)	132(4)
C(2)	2156(10)	0	1504(54)	184(11)
F(1)[b]	547(16)	3803(27)	6385(35)	137(8)
F(1′)[b]	640(20)	3674(20)	5262(34)	132(6)
F(2)[b]	198(21)	5000	2508(48)	137(8)
F(2′)[b]	752(15)	5000	3274(41)	115(7)

[a] *U*(eq) is defined as one-third of the trace of the orthogonalized $\mathbf{U}_{ij}$ tensor. [b] Occupancy factor, 0.5.

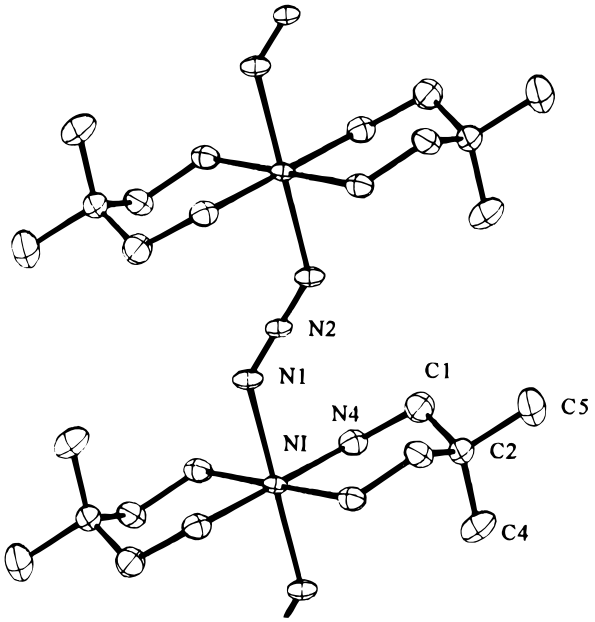

Figure 1. Atom labeling scheme of the cationic part of [Ni(1,3-diamino-2,2-dimethylpropane)$_2$(μ-N$_3$)]$_n$(PF$_6$)$_n$ (**1**).

[Ni(1,3-diaminopropane)$_2$(μ-N$_3$)]$_n$(PF$_6$)$_n$ (2). A labeled scheme is shown in Figure 2. The crystal packing is given in Figure 3. The main bond lengths and angles are listed in Table 3. Other distances and angles may be found in the Supporting Information. The nickel atom occupies a distorted octahedral environment, formed by two N atoms of the azido bridging ligands at 2.122 Å and four N atoms of the two bidentate amine ligands at the same distance, 2.100 Å, giving a local D_{4h} symmetry. The most important data from magnetic point of view are the Ni−N(1)−N(2) angle and the dihedral Ni−NNN−Ni torsion angle. These angles are 126.1 and 0°, respectively.

Modification of the Structures at Low Temperature. The susceptibility measurements for **1** and **2** (see below**)** indicate an abrupt change of χ_M values at 235 and 230 K, respectively.

Table 3. Selected Bond Lengths (Å) and Angles (deg) for **1** and **2**[a]

	1	**2**
Ni−N(1)	2.125(3)	2.122(8)
Ni−N(4)	2.108(3)	2.100(6)
N(1)−N(2)	1.157(4)	1.201(10)
N(1)^1−Ni−N(1)	180.0	180.0
N(1)−Ni−N(4)	92.12(12)	91.8(3)
N(1)−Ni−N(4)^1	87.88(12)	88.2(3)
N(1)^1−Ni−N(4)	87.88(12)	88.2(3)
N(1)^1−Ni−N(4)^1	92.12(12)	91.8(3)
N(4)^1−Ni−N(4)	87.9(2)	87.6(4)
N(2)−N(1)−Ni	136.5(3)	126.1(8)
N(1)−N(2)−N(1)^2	180.0	180.0

[a] Symmetry transformations used to generate equivalent atoms for **1** and **2** (indicated with superscript number on atom): (1) $-x, y, -z$; (2) $-x, -y, 1 - z$.

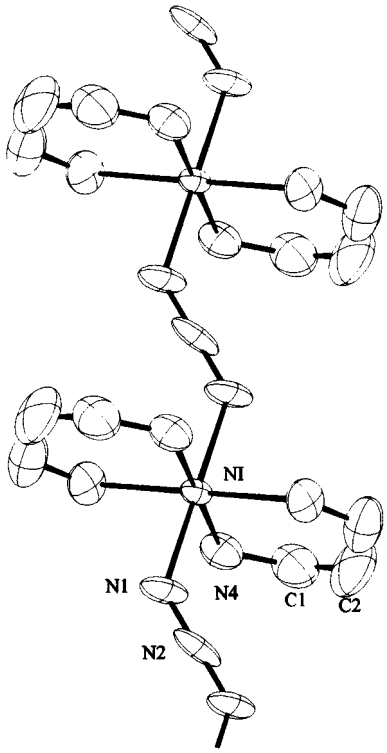

Figure 2. Atom labeling scheme of the cationic part of [Ni(1,3-diaminopropane)$_2$(μ-N$_3$)]$_n$(PF$_6$)$_n$ (**2**).

Indeed, we repeatedly attempted to solve the crystal structure at these moderate temperatures, but, unfortunately, all of the crystals of both complexes lost their crystallinity, which made it impossible to resolve the crystal and molecular structure. For this reason we decided to study the possible changes in the crystal net by X-ray powder diffraction on the two new complexes. In both cases, the crystal parameters *a*, *b* change but *c* remains practically constant and one of the angles becomes different to 90° (orthorhombic → monoclinic). These variations are shown in Table 4 and Figures 4 and 5. As can be observed from these data, the *a* parameter for complex **1** increases from approximately 18.0 to 18.8 Å, the *b* parameter decreases from 8.65 to 8.11 Å, and *c* parameter, along which the chain runs, is practically invariable. The β angle increases from 90 to 91.5°. These changes take place between −25 and −50° (Figure 4). This process is completely reversible, without a hysteresis loop. In contrast, for **2** (Figure 5), very similar changes are observed but with a hysteresis loop. The *a* parameter decreases with lower temperature from approximately 15.2 to 15.0 Å; *b* parameter has a less pronounced decrease, from 8.8 to 8.6 Å, *c* parameter, along which the chain runs, is practically invariable,

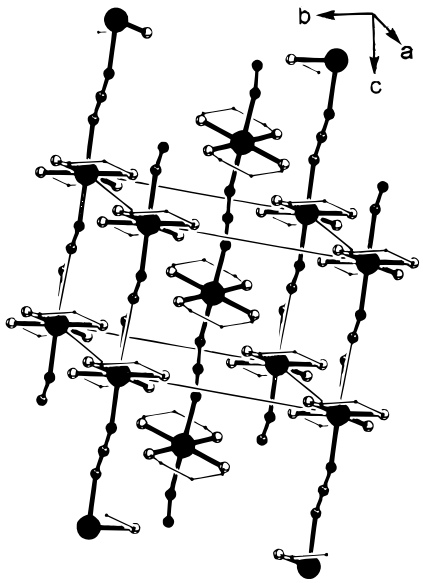

Figure 3. Plot of the crystal packing for [Ni(1,3-diaminopropane)$_2$-(μ-N$_3$)]$_n$(PF$_6$)$_n$ (**2**).

Table 4. Thermal Variation for Cell Parameters from X-ray Powder Diffraction

Compound **1**

T (K)	a (Å)	b (Å)	c (Å)	β (deg)
298	18.092	8.647	6.153	90.0
273	18.067	8.637	6.147	90.0
248	18.025	8.632	6.141	90.0
223	18.775	8.133	6.168	91.39
198	18.733	8.122	6.167	91.53
173	18.706	8.129	6.161	91.16
158	18.687	8.117	6.163	90.97

Compound **2**[a]

	a (Å)		b (Å)		c (Å)		β (deg)	
T (K)	↓	↑	↓	↑	↓	↑	↓	↑
298	15.220	15.214	8.800	8.801	5.937	5.933	90.0	90.0
273	15.181	15.184	8.793	8.788	5.918	5.917	90.0	90.0
248	15.156	15.005	8.769	8.663	5.905	5.929	90.0	91.93
223	15.150	14.998	8.739	8.691	5.896	5.893	90.0	92.42
198	14.962	14.990	8.665	8.640	5.891	5.911	92.40	92.82
173	14.954	14.918	8.668	8.610	5.927	5.921	92.39	92.62
158	14.964	14.964	8.650	8.650	5.914	5.914	92.98	92.98

[a] ↓, lowering temperature; ↑, increasing temperature.

and, finally, β parameter changes from 90 to 93°. These variations are reversible, giving a hysteresis loop, as shown in Figure 5. From these data, it is important to point out that if c parameter is constant at any temperature and the chains run along this axis, the Ni−N−N angles (very important from a magnetic point of view) should be maintained constant. The variation takes place only in a and b parameters, deforming the cell in the direction perpendicular to the chains, creating, indeed, a necessary variation in the dihedral Ni−NNN−Ni angle, also very important from the magnetic point of view. Taking into account that this Ni−NNN−Ni torsion angle is 0° at room temperature (ideal value for maximum antiferromagnetic coupling), any deformation in the cell creates a Ni−NNN−Ni torsion angle different from 0°, consequently decreasing the coupling J values.

To complete this work in the powder complexes, DSC measurements were carried out from room temperature to −100°. For **1** there is an endothermic peak, sharp, with the onset temperature at −44.0 °C (on cooling) and at −38.44 °C (on heating) with ΔH = 0.024 J/mol. For **2** this peak is very

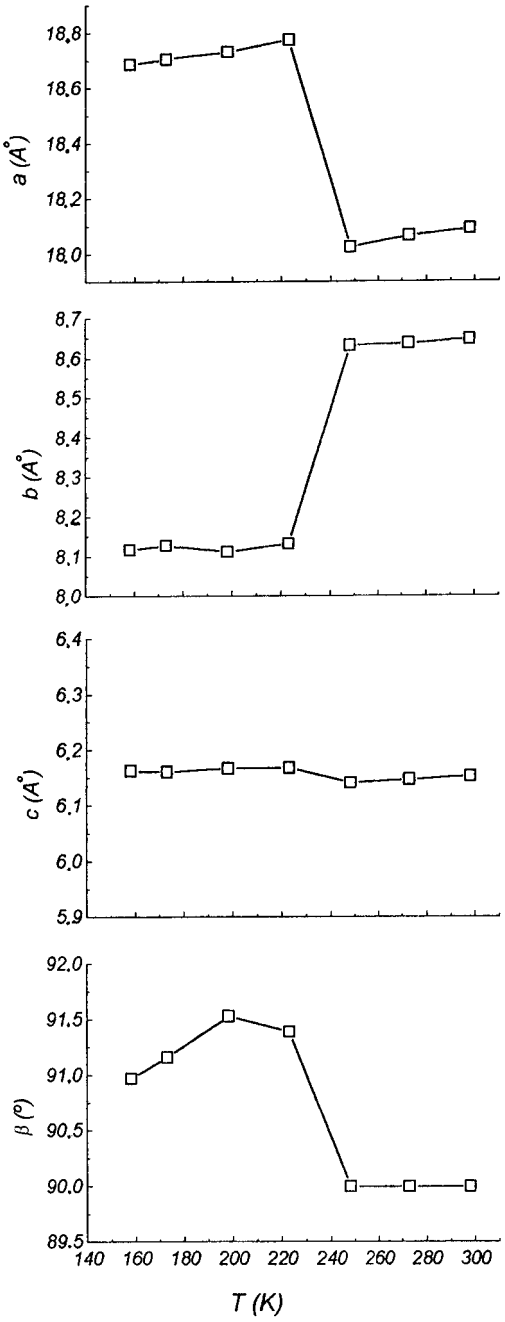

Figure 4. Variation of the cell parameters with temperature for [Ni-(1,3-diamino-2,2-dimethylpropane)$_2$(μ-N$_3$)]$_n$(PF$_6$)$_n$ (**1**).

broad with the onset temperature at −51.3 °C (on cooling) and at −54.0 °C (on heating); ΔH = 0.009 J/mol. These results (X-ray powder diffraction and DSC measurements) confirm that there is a phase transition in the two complexes at relatively high temperature. The low changes in the crystal parameters and the low values of ΔH indicate that the changes in the transition temperature are small.

Magnetic Properties. The molar magnetic susceptibilities for **1** and **2** are plotted in Figure 6. For **1**, the molar susceptibility value (3.15×10^{-3} cm^3 mol^{-1} at 320 K) increases when the temperature decreases, presents a clear change at 230 °C, and then continues increasing to a maximum of 1.1×10^{-2} cm^3 mol^{-1} at 35.1 K, and below this temperature the curve decreases continuously to 6.6×10^{-3} cm^3 mol^{-1} at 4 K. For **2**, the behavior is similar: the molar susceptibility value (2.9×10^{-3} cm^3 mol^{-1} at 300 K) increases when the temperature decreases, presents a clear change at 230 °C, and then continues to increase to a maximum of 4.2×10^{-3} cm^3 mol^{-1} at 100 K,

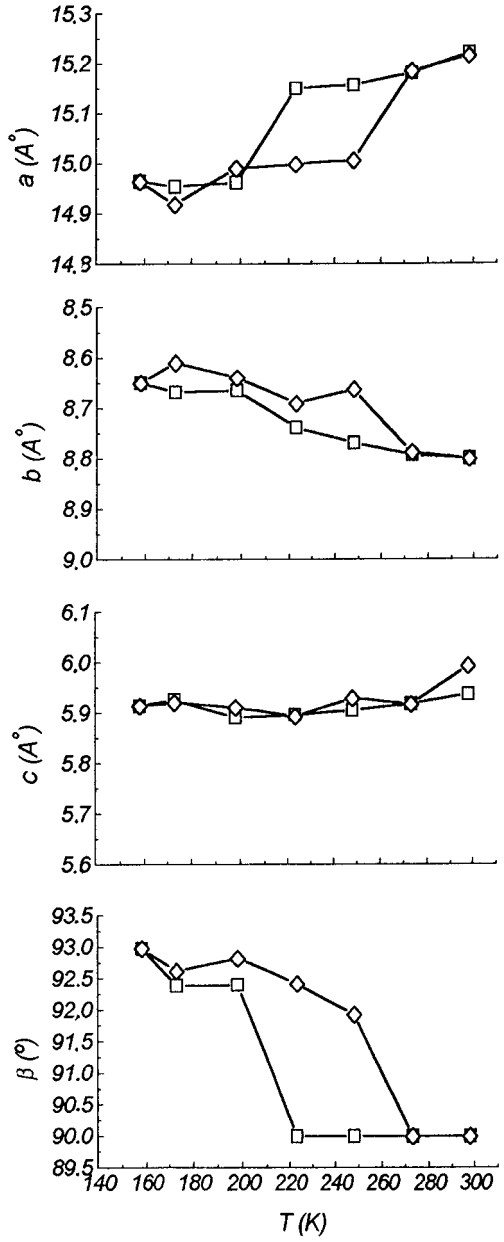

Figure 5. Variation of the cell parameters with temperature for [Ni(1,3-diaminopropane)$_2$(μ-N$_3$)]$_n$(PF$_6$)$_n$ (**2**): (◇, heating; □, cooling).

and below this temperature the curve decreases continuously to 1.8×10^{-3} cm^3 mol^{-1} at 4 K. Accurate susceptibility measurements in the discontinuity interval (Figure 7) show hysteresis loops for both complexes. For **1** this hysteresis loop is given in an interval lower than 10° (between 230 and 240 K approximately), whereas for complex **2** this hysteresis loop is more pronounced: the interval is approximately 50° (between 210 and 260 K). This may explain why in X-ray powder diffraction (see above) the hysteresis loop was observed only for compound **2**. This behavior was also observed in some dinuclear complexes with the bridging azido group in end-on coordination mode.[11]

The most general spin Hamiltonian to describe the magnetic properties of isotropic Ni(II) chains, taking into account the single-ion terms and the interactions between the nearest-neighbor centers is

$$H = \Sigma(\beta S_i g_i H - J S_i S_{i+1})$$

The terms corresponding to the anisotropic and antisymmetric

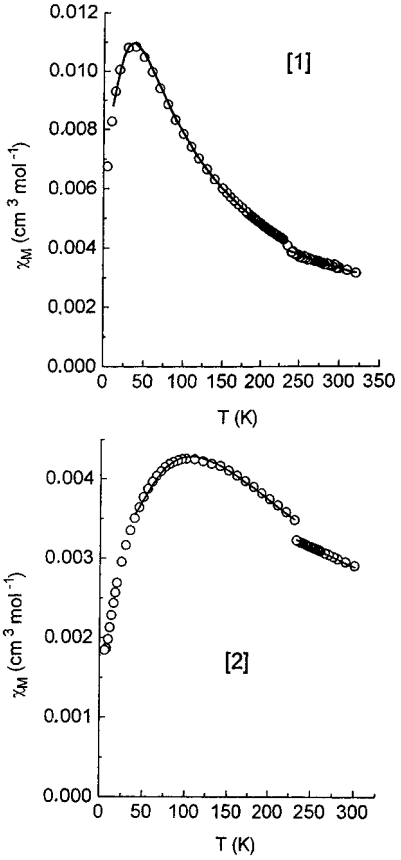

Figure 6. Magnetic susceptibility plots of polycrystalline samples for [Ni(1,3-diamino-2,2-dimethylpropane)$_2$(μ-N$_3$)]$_n$(PF$_6$)$_n$ (**1**) and [Ni(1,3-diaminopropane)$_2$(μ-N$_3$)]$_n$(PF$_6$)$_n$ (**2**). Solid lines show the best fits (see text).

exchange have not been considered because these effects are relevant only at very low temperatures.

There is no exact mathematical expression for χ_M *vs* T of infinite Heisenberg chains. Nevertheless, there are numerical calculations that approximately characterize the Heisenberg behavior for 1-D systems.[29,30] In the case of isotropic 1-D $S = 1$ systems the temperature dependence of the susceptibility extrapolated from calculations performed on ring systems of increasing length has been given by Weng.[31] Our experimental data were then fitted to the Weng equation

$$\chi_M = \frac{N\beta^2 g^2}{kT} \frac{2 + 0.019\alpha + 0.777\alpha^2}{3 + 4.346\alpha + 3.232\alpha^2 + 5.83\alpha^3}$$

where $\alpha = |J|/kT$.

This formula is valid only for antiferromagnetic coupling and only if the nickel ion is magnetically isotropic. A good fit is possible only down to a temperature near the maximum of χ_M because neither zero-field splitting nor the Haldane gap effect[32] is taken into account in the equation. The J values were obtained by minimizing the function $R = \Sigma(\chi_M^{calc} - \chi_M^{obs})^2/\Sigma(\chi_M^{obs})^2$.

For **1** and **2**, taking into consideration the change in the magnetic susceptibility measurements at low temperature, we

(29) Blöte, H. W. *J. Am. Chem. Soc.* **1964**, *32*, 343.
(30) De Neef, T.; Kuipers, A. J. M.; Kopinga, K. *J. Phys.* **1974**, *A7*, L171.
(31) Weng, C. Y. Ph.D. Thesis, Carnegie Institute of Technology, 1968.
(32) (a) Haldane, F. D. M. *Phys. Rev. Lett.* **1983**, *50*, 1153. (b) Haldane, F. D. M. *Phys. Lett.* **1983**, *93A*, 464. (c) Renard, J. P.; Verdaguer, M.; Regnault, L. P.; Erkelens, W. A. C.; Rossat-Mignon, J.; Stirling, W. G. *Europhys. Lett.* **1987**, *3*, 945. (d) Renard, J. P.; Verdaguer, M.; Regnault, L. P.; Erkelens, W. A. C.; Rossat-Mignon, J.; Ribas, J.; Stirling, W. G.; Vettier, C. J. *Appl. Phys.* **1988**, *63*, 3538.

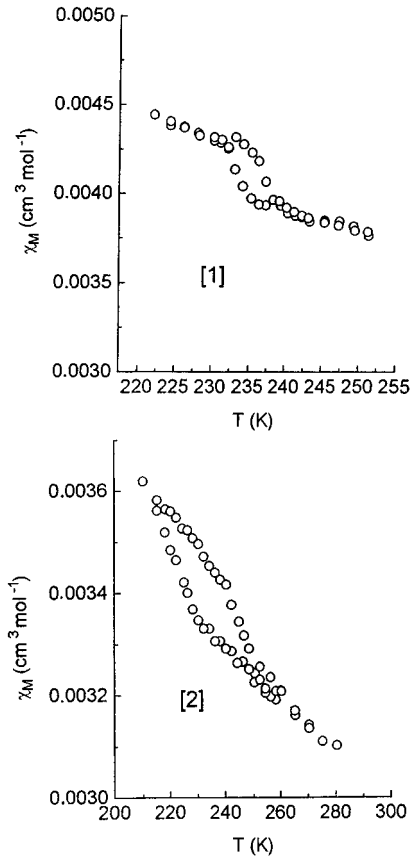

Figure 7. Hysteresis loop for [Ni(1,3-diamino-2,2-dimethylpropane)$_2$-(μ-N$_3$)]$_n$(PF$_6$)$_n$ (**1**) and [Ni(1,3-diaminopropane)$_2$(μ-N$_3$)]$_n$(PF$_6$)$_n$ (**2**).

made two fittings to calculate J values separately: one in the high-temperature region (before the susceptibility change) and another in the low-temperature zone (after the susceptibility change). The best-fitted parameters so obtained are as follows: $J = -41.1$ cm^{-1}, $g = 2.29$, and R $= 2.0 \times 10^{-6}$ for **1** and $J = -70.6$ cm^{-1}, $g = 2.36$, and $R = 6.6 \times 10^{-6}$ for **2** (high-temperature zone); $J = -19.4$ cm^{-1}, $g = 2.16$, and R $= 2.9 \times 10^{-5}$ for **1** and $J = -55.8$ cm^{-1}, $g = 2.29$, and $R = 2.9 \times 10^{-5}$ for **2** (low-temperature zone).

Interpretation of the Magnetic Results. In previous studies magnetostructural correlations in end-to-end *trans*- and *cis*-azidonickel(II) chains have been reported.[13,17] The three main factors are the Ni−N−N angles, the Ni−NNN−Ni torsion angle, and the Ni−N(azido) distances. For the Ni−N−N angle, molecular orbital calculations showed that the maximum coupling is expected for $\alpha = 108°$. For greater α values the antiferromagnetic interaction must decrease (as found experimentally) with an accidental orthogonality valley centered at $\alpha = 165°$. The effect of the Ni−NNN−Ni torsion angle was also parametrized. For all α values, the maximum coupling can be expected for a torsion angle of zero, decreasing gradually when the torsion angle increases. The magnitude of this effect is lower than the effect of the bond angle. Finally, calculations varying d (Ni−N distance) in the range 2.00−2.20 Å indicate that, for greater distances, lower antiferromagnetic values occur.

Consequently, for the high-temperature region in which the molecular stucture is solved, the differences in these three factors for **1** and **2** are as follows**:** the Ni−N(azido) distances are the same (2.12 Å), the Ni−NNN−Ni torsion angle is 0° in both cases, and the only remarkable difference lies in the Ni−N−N angle: 136.5° for **1** and 126.1° for **2**. This difference explains that J is lower for **1** (-41.1 cm^{-1}) than for **2** (-70.6 cm^{-1}). When the temperature is decreased, according to the studies made by X-ray powder diffraction (see above) the only parameter that may change is the Ni−NNN−Ni torsion angle. Taking into account that at room temperature we are in the most ideal conditions for antiferromagnetic coupling (torsion = 0°), any change must decrease the antiferromagnetic coupling, as is observed experimentally.

Acknowledgment. We are very grateful for the financial assistance from the CICYT (Grant PB93-0772) and to Dr. Nuria Clos for technical assistance with the magnetic measurements.

Supporting Information Available: Tables giving crystal data and details of the structure determination, anisotropic thermal parameters, bond angles and distances, and hydrogen atom coordinates (7 pages). Ordering information is given on any current masthead page.

IC960733D